ELSEVIER

Contents lists available at ScienceDirect

Journal of Membrane Science

journal homepage: www.elsevier.com/locate/memsci



A geometric model to predict protein retentions during skim milk microfiltration

Hilda Lucy Nyambura ^{a,*}, Anja E.M. Janssen ^a, Albert van der Padt ^{a,b}, Remko M. Boom ^a

- ^a Food Process Engineering Group, Wageningen University & Research, P.O. Box 17, 6700AA, Wageningen, the Netherlands
- ^b FrieslandCampina, Stationsplein 4, 3818 LE, Amersfoort, the Netherlands

ARTICLE INFO

Keywords:
Milk protein microfiltration
Casein micelle
Interfacial tension
Geometric model

ABSTRACT

Microfiltration membranes can retain dissolved proteins to some degree, as result of interactions with other components. This work presents a geometric model to describe the limiting transmembrane pressure, flux, and the transmission of dissolved proteins. The effects of temperature and membrane pore size are observed in other factors such as viscosity, membrane resistance and rate of mass transfer. The model could predict the experimental transmembrane flux values at different temperatures. With a decrease in temperature from 15 °C to 5 °C, the viscosity increased from 1.6 mPa s to 2.2 mPa s while the rate of mass transfer decreased with decreasing temperature of the same range from 0.9×10^{-6} m s⁻¹ to 2×10^{-6} m s⁻¹. With a change in temperature, there was insignificant difference between the transmission of whey proteins. The same was observed with different pore sizes. This confirmed the hypothesis that the concentration polarization layer that determines the protein transmission being a sieving layer at pressures higher than the limiting transmembrane pressure.

1. Introduction

Bovine milk comprises of several proteins, classified into casein and whey proteins that have different functional and nutritional properties. Caseins are traditionally mostly used to produce cheese while whey proteins have many applications e.g. in sports and elderly nutrition [1]; [2-5]. Therefore, separating these fractions is crucial for the dairy industry. One of the commonly used methods of separation of different components in bovine milk is crossflow microfiltration [6,7]. This is possible since caseins tend to be aggregated in micelles larger than approximately 100 nm, while whey proteins typically are mostly molecularly dissolved [8]; [7,9,10]. An advantage of microfiltration process is that products remain in their native form since no chemicals are added to the process. There are different types of microfiltration membranes used in industry with polymeric membranes gaining popularity over the years as compared to ceramic membranes [1]; [5,11–13]. Even though ceramic membranes have higher fluxes in comparison to polymeric membranes, polymeric membrane modules can have higher membrane surface area and be cost effective [14]. Hence, polymeric spiral wound membranes are preferred for this reason.

The choice of the membrane pore sizes, the material of the polymeric

membrane, the module configuration and the operation conditions such as temperature all affect the separation efficiency [15,16]. At high processing temperatures of 50 °C, bovine milk microfiltration can give a permeate with a high serum protein content with essentially no caseins. Lower filtration temperatures of 10 °C and below, produce a permeate with whey proteins that are enriched with β -casein [16,17] and bacterial growth is curbed [9]. While giving poorer separation lower temperatures offer other advantages such as flux stability during extended fractionation periods and reduced fouling due to lower release of calcium phosphate and reduced denaturation of proteins [12,15]. Other studies showed that cheese produced from the retentate having reduced β -case in improved the spreadability during melting and was found to be less bitter due to slower release of peptides during aging [18]. However, lower temperatures also result in a lower transmembrane flux due to increase in viscosity, thus increasing processing costs. At the same time, whey proteins show some retention during microfiltration of milk, which may lead to suboptimal separation if not considered.

While most studies in this field have been experimental, several models have been created to predict the transmembrane flux to further understand the mechanism of skim milk crossflow microfiltration [19, 20]. Bacchin et al. developed a model for mass accumulation from a

E-mail addresses: hilda.nyambura@wur.nl (H.L. Nyambura), anja.janssen@wur.nl (A.E.M. Janssen), albert.vanderpadt@wur.nl (A. van der Padt), remko.boom@wur.nl (R.M. Boom).

^{*} Corresponding author.

polarized layer to a fully formed deposit layer during filtration using ultrafiltration membranes. They accounted for the properties of the suspension using osmotic pressure and compression resistance [21]. Additionally, description of the formation of a deposit layer during skim milk filtration has been described [22]. However, these approaches used dead end filtration and only described the effect this has on flux and behavior of membrane deposit in relation to pressure and filtered volume. Gebhardt, using both microfiltration and ultrafiltration membranes, investigated the effect that the filtration forces have on the casein micelle [23]. When these micelles are deposited on the membrane surface, they negatively affect the filtration process, and this is majorly due to the change in structure of the micelle. With increased transmembrane pressure, the shape of the micelles change from spherical to an oblate structure [23]. The effect of this change of shape on retention of other milk proteins during filtration has not been investigated. Bouchoux et al. used a milk example to provide a general approach for predicting the filtration of soft, deformable and permeable colloids [24]. They built a filtration model based of osmotic pressure and hydraulic permeability. This model can predict flux and concentration of the casein micelles in the deposit layer. The findings were that the concentration of casein micelles increases towards the membrane surface and this negatively affect the permeate flux since the compression of these micelles reduces the permeability of this layer [24]. These researchers have demonstrated that casein micelles are soft and deformable, and this has a negative effect on the flux. Further, Opong and Zydney [25], using a stirred ultrafiltration device evaluated the transport of bovine serum albumin through asymmetric polyether sulfone ultrafiltration membrane with different molecular weight cutoff Opong & Zydney, 1991. With this evaluation, they presented results of a hydrodynamic model for the hindrance factors for convective and diffusive transport of spherical solutes through well-defined pores with the effective solute to pore size ratio evaluated from a partitioning model. Their model accounted for the ellipsoidal shape of the protein and the membrane pore size pores size distribution. The results of the model were in agreement with the results of the conducted experiment Opong & Zydney, 1991. Boyd and Zydney [26] extended the model presented by Opong and Zydney [25] to include solute transport through a multilayer membrane with emphasis on physical basis for the complex transport properties [26]. For this they used ultrafiltration membranes with different molecular weight cut offs (30 and 50 kD) stacked on to each other (in series) forming multilayers to evaluate the sieving of dextran. They found that the sieving characteristics of these multilayer membranes are dependent on the properties and orientation of the different layers [26]. These two models were based on dead end filtration and do not include the effect of the change in the pore size of either when evaluated individually or when in multilayer format.

To the best of our knowledge, no models are available to predict the transmission of dissolved bovine milk proteins during microfiltration of milk that considers the behavior of casein micelles during the filtration process. During fractionation, casein micelles are retained by the membrane since they are bigger in size compared to the pores of the membrane. Due to this retention, a concentration polarization layer develops and increases with an increase in transmembrane pressure [27]. This layer acts as a dynamic membrane on top of the microfiltration membrane and is responsible for the transmission of the dissolved proteins [28]; [29]. The transmembrane pressure that is applied during filtration deforms the accumulated micelles from spherical shape to a different structure and this reduces the permeability of this layer. Reduced permeability would result in a decreased transmission of soluble proteins.

This work therefore proposes a simple geometric model to predict the transmembrane flux and transmission of soluble proteins during microfiltration of skim milk. The model will be compared to experimental data, with respect to the permeation behavior of casein and whey proteins α -lactalbumin, β -lactoglobulin and immunoglobulin M (α -la, β -Lg, and IgM, respectively) at different transmembrane pressures,

temperatures, and pore sizes.

2. Materials and methods

2.1. Experimental design

Polymeric spiral wound microfiltration membranes were used to conduct skim milk fractionation. Table 1 summarizes the membrane types and manufacturers. A microfiltration membrane with an average pore size of 0.1 μm was used to investigate the effect of temperature on skim milk fractionation at 5, 10, and 15 °C. To evaluate the effect of membrane pore size, additional runs at 10 °C were done with membranes having 0.2 and 0.3 μm nominal pore size. Skim milk was delivered 24 h prior to the experiments and stored at 4 °C. All experiments were conducted in duplicates; each set of duplicates was done with skim milk from a single batch.

2.2. Skim milk

Pasteurized skim milk was purchased from Jumbo supermarket with its original source from a FrieslandCampina factory in Rotterdam, The Netherlands. The pasteurization process is done in the factory at 72 $^{\circ}\text{C}$ for 20 s before being packaged and distributed to supermarkets.

2.3. Membrane installation

Microfiltration was performed using a pilot scale membrane filtration unit as described by Ref. [30,31] with the schematic diagram as shown in Fig. 1. The membrane unit was equipped with a plate heat exchanger for temperature control between 5 and 15 $^{\circ}$ C at intervals of 5 $^{\circ}$ C. Several microfiltration membranes as shown in Table 1 were used. The operation transmembrane pressures varied between 0.2 and 3 bar. All experiments were conducted at a crossflow velocity of 0.16 m/s in recirculation mode. An equilibration time of 45 min was allowed at each of the specific temperatures and transmembrane pressure to ensure stable conditions during recirculation mode.

2.4. Cleaning procedure

After flushing out the skim milk with water, an enzymatic cleaning was conducted using a solution of Divos 90 at 1 % (v/v) and Divos 80–2 at 0.35 % (v/v) respectively. This solution was recirculated for 40 min at a temperature of 50 °C. Rinsing was done using tap water to a neutral pH at a temperature not higher than the cleaning temperature. Acidic cleaning followed using Divos 2 at 0.5 % (v/v) for 20 min at a temperature of 50 °C. This was followed by rinsing using tap water until neutral pH is achieved. The last step was alkaline cleaning using Divos 116 at 0.8 % (v/v) for 25 min at 50 °C. After rinsing out the alkaline cleaning

Table 1 Geometric and hydrodynamic properties of membranes used for skim milk fractionation as provided by the membrane manufacturer. Water permeability was measured using the pilot scale membrane filtration unit. Overall, there was $1{\text -}10~\%$ loss in permeability after membrane cleaning.

Characteristics							
Membrane Producer	Suez GE	Synder	Synder				
		Filtration	Filtration				
Type number	1812 JX	1812 V0.2	1812 V0.1				
Polymer	PVDF	PVDF	PVDF				
Pore Size (µm)	0.3	0.2	0.1				
Membrane Diameter (m)	0.046	0.046	0.046				
Membrane Length (m)	0.3	0.3	0.3				
Active Area (m ²)	0.38	0.334	0.334				
Spacer thickness (m)	8.128×10^{-4}	7.874×10^{-4}	7.874×10^{-4}				
Water Permeability (lm $^{-2}$ h $^{-1}$ bar $^{-1}$) at 10 $^{\circ}$ C	105 ± 8	94 ± 4	85 ± 11				

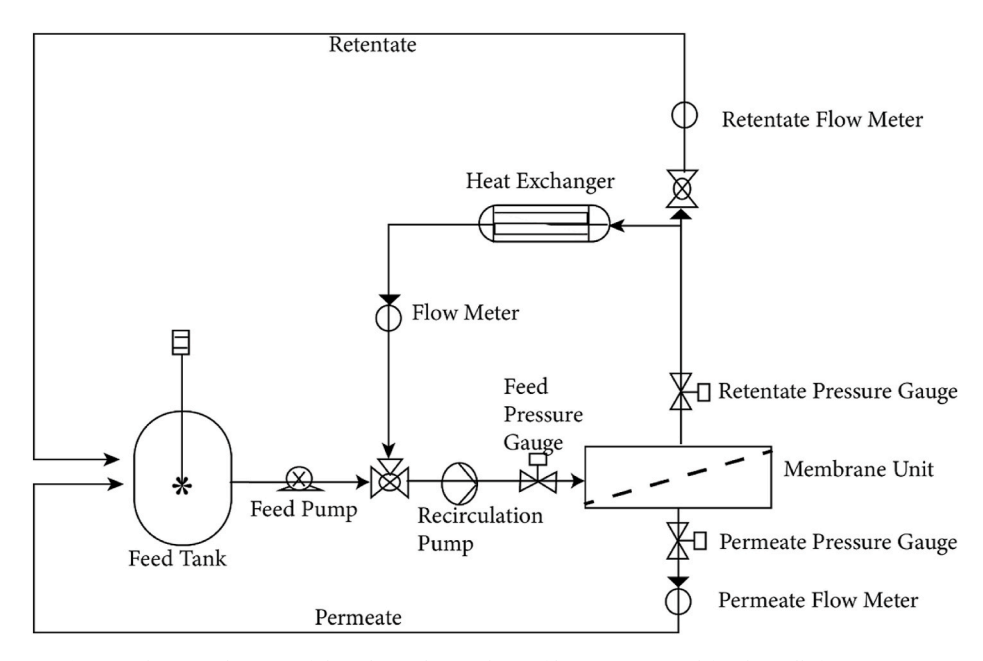


Fig. 1. Schematic drawing of the pilot scale membrane filtration unit used for the milk fractionation.

compound, a clean water flux experiment is conducted using demineralized water to assess the effectiveness of cleaning. The clean water fluxes for each membrane are as shown in Table 1. All Divos cleaning agents were purchased from Diversey, The Netherlands.

2.5. Casein, serum protein and viscosity analyses

The analysis of casein and serum protein was done using High Performance Size Exclusion Chromatography (HPSEC), using two columns in series namely TSK G400SWxl 7.8 \times 300 mm, 8 μm and TSK 53000SWxl 7.8 \times 300 mm, 5 μm by Tosoh Bioscience. The mobile phase applied consisted of 0.01 % Trifluoroacetic acid (TFA) in 69.9 % High Performance Liquid Chromatography (HPLC) grade water and 30.0 % Acetonitrile (ACN). The flow rate was 1.5 ml/min, the column temperature was kept at 30 °C and detection was done at a UV wavelength of 215 nm. For the analysis of whey proteins, the casein was precipitated by adding 2 M hydrochloric acid and centrifugating at 7600 g for 10 min. The supernatant was then analyzed using the abovementioned columns, eluents, and operation conditions. HPSEC calibration was done using casein and serum protein standards to aid in calculation of the actual concentration of casein and serum protein (see Appendix figure A.4 and A.5).

The viscosity of skim milk and samples collected during filtration were measured using an Anton Paar Rheometer MCR502 with a double gap geometry at the temperatures of 5 $^{\circ}$ C, 10 $^{\circ}$ C and 15 $^{\circ}$ C.

2.6. Calculations

The transmembrane pressure (Δp_{tm}) was defined using Equation (2.1).

$$\textit{Transmembrane pressure} = \left[\frac{P_f + P_r}{2}\right] - P_p \tag{2.1}$$

Where P_f , P_r , and P_p are the measured/set point pressures in the feed, retentate and permeate side of the membrane.

The transmission of a protein (T) was calculated using concentrations in the permeate (C_p) and retentate (C_r) as shown in Equation (2.2).

$$T(\%) = \frac{C_p}{C_r} \times 100 \tag{2.2}$$

The transmembrane flux (\overline{u}) was calculated from the permeate flow

rate ($\dot{V}_{permente}$) and the membrane area as shown in Equation (2.3).

$$\overline{u} = \frac{\dot{V}_{permeate}}{Membrane Area}$$
 (2.3)

The mass flux of a protein, another measure of filtration performance of the membranes, was calculated by multiplication of the volumetric transmembrane flux and the concentration of each protein in the permeate as shown in Equation (2.4).

$$Mass Flux = \overline{u} \times C_p \tag{2.4}$$

3. Modelling framework

The model is based on several observations during filtration of skim milk. During filtration of skim milk, casein micelles are retained by the membrane to a larger extent as compared to the serum proteins. In order to explain the effect that these micelles have on filtration, a geometric model is developed.

3.1. Model assumptions

3.1.1. Development of the concentration polarization layer

In the development of this model, several assumptions are made. The first set of assumptions are based on the development of the concentration polarization layer that consists of mainly casein micelles. It is assumed that filtration results in retaining and concentrating casein micelles near the membrane surface, and this is termed as concentration polarization. The second assumption is that an increase in transmembrane pressure results in the increase of casein micelles on the membrane surface. The third assumption is that at a given critical transmembrane pressure, the first layer of micelles on the membrane surface reaches the concentration of the hexagonal close packing referred to as the developed concentration polarization layer. The fourth assumption is that further increase in transmembrane pressure above the critical transmembrane pressure results in compression of the casein micelles in the developed concentration polarization layer. However, the compressed casein micelles on the very first layer next to the membrane surface maintain the hexagonal close packing.

3.1.2. Casein micelle layer structure and distribution over the membrane surface

Since microfiltration of skim milk is a pressure driven process, transmembrane pressure is increased to obtain permeate. It is assumed that when the applied transmembrane pressure reaches a critical value, the developed casein micelle layer appears and covers the entire membrane surface. Upon further increase of this pressure above the critical value, it is assumed that the casein micelle layer that covers the entire membrane surface is compressed uniformly along the membrane surface. Lastly this compressed layer is assumed to remain stagnant after it is formed [32].

3.1.3. Transmission of proteins

Since the goal of microfiltration of skim milk is to obtain the two distinct fractions of proteins (micellar casein and serum protein) separately, evaluation of transmission of serum protein is essential. To evaluate this transmission, several assumptions are made in order to develop this geometric model. It is assumed that both the membrane pores and the pores in between the casein micelles referred to as interstitial pores can retain serum proteins and reduce their transmission into the obtained permeate. In description of transmission of serum proteins, only size exclusion based on the protein size and the pore size will be taken into account. The sizes of serum proteins are as follows: β-lg has a diameter of 3.5–4.2 nm, α -lg has a diameter of 1–2.5 nm and IgM has a diameter of 25-37 nm and are assumed to be hard spheres [33-35]. Casein micelles at a pH of 6.7 are assumed to be monodispersed, soft and deformable spheres which are much larger in size with an average diameter of 250 nm [36]; [37,38]. All other possible interactions not related to size exclusion will be neglected. In our approach, we assume that approach by Ferry is sufficient in description of resulting serum protein transmission from size exclusion. We can understand this by considering that for a molecule of a known size in a pore with a known radius, simple geometric exclusion from the membrane pore would lead to an a given transmission or exclusion factor [39] (equation (3.1)).

$$\Phi = \left(1 - \frac{r_s}{r_n}\right)^2 \tag{3.1}$$

In our case the exclusion factor for a pore of 0.2 μm would be 0.67 to 0.96, leading to a moderate intrinsic retention by the membrane alone (equation (3.1)). The transmission of serum proteins can therefore be described as (equation (3.2)):

$$\frac{C_p}{C_m} = T_r \tag{3.2}$$

Equation (3.2) holds true that the membrane is responsible for sieving when the applied transmembrane pressure is below the critical transmembrane pressure. Based on this, it is therefore assumed that below the critical transmembrane pressure, the size of the interstitial pores in the less developed concentration polarization layer is too large to effect any retention of serum proteins. Hence only equation (3.2) is applicable in the description of serum protein transmission. As earlier stated, the transmembrane pressure is increased to have a positive effect on permeate. Therefore, when the transmembrane pressure is increased above the critical point, it is assumed that the resulting compressed casein micelle layer begins to impact the transmission of serum protein. Additionally, it is only the very first layer of this compressed casein micelle layer which is next to the membrane that impacts the serum protein transmission. The last assumption is that the total transmission of serum protein across fully developed concentration polarization layer and the membrane is the product of transmission across this layer and the transmission across the membrane. This assumption is applicable when the transmembrane pressure is above the critical transmembrane pressure.

3.2. Model development

With the stated assumptions, a geometric model is developed for the decrease in transmission at larger fluxes. During filtration process, both the developed concentration polarization layer and the membrane offer resistance to the transmission of proteins. At the beginning of this filtration process with positive but minimal application of pressure, only membrane resistance is significant. This is because the concentration polarization layer has not fully developed and the interstitial pores in between the casein micelles are relatively large (Fig. 2) to offer any retention. Calculation of the size of the interstitial pores can be done taking into account only three spheres in contact [40].

$$A = A_T - A_C = r^2 \left(\sqrt{3} - \frac{1}{2}\pi\right) \approx 0.161 \, r^2$$
 (3.3)

These pores have a triangular shape. We do not know what influence the shape of the pores has on the transmission of any molecule, and therefore we convert the cross-sectional area into an equivalent hydraulic diameter using equation (3.4):

$$d_h = \frac{4A}{P} \tag{3.4}$$

Where P is equal to πr for a triangle made up of three parts of a sixth of a circle (see Fig. 2a). This leads to

$$d_h = \frac{4r^2\left(\sqrt{3} - \frac{1}{2}\pi\right)}{\pi r} = r\left(\frac{4}{\pi}\sqrt{3} - 2\right) \approx 0.205 \ r = 0.103 \ d_{cas}$$
 (3.5)

For an estimated d_{cas} of 250 nm, with transmembrane pressure below critical transmembrane pressure, the typical interstitial pore size would be 25 nm. This is too large to induce any retention of dissolved milk proteins and implies that the smaller proteins such as β -lg, α -lg and IgM can have significant transmission through this layer.

As soon as there is increase in pressure, the soft casein micelles deform and compress onto each other [41]; [5], resulting in smaller interstitial pores, like a draining foam (see Fig. 2b). Geometric considerations then show us that the resulting pore area can be described using equation (3.6).

$$A = \left(\sqrt{3} - \frac{1}{4}\pi\right)r_d^2\tag{3.6}$$

Therefore, r_d is smaller than the radius of the micelles, due to the compression. The pressure that causes the compression and the resulting r_d are related by the Laplace pressure, which in this case is $\Delta p = \gamma/r_d$ (the relevant pores are tubelike pores between three micelles, so there is only one curvature). Th $is\ \Delta p$ is created by the pressure gradient over the layer of casein micelles on the membrane; γ is the measure of energy that is required to deform a casein micelle such that its surface area increases [42]. This gives then for the cross-sectional pore area:

$$A = \left(\sqrt{3} - \frac{1}{4}\pi\right)r_d^2 = \left(\sqrt{3} - \frac{1}{4}\pi\right)\left(\frac{\gamma}{\Delta p}\right)^2 \tag{3.7}$$

We can now derive the equivalent r_h of such a pore by using equation (3.8).

$$r_{h} = \frac{2A}{P} = \frac{\left(2\sqrt{3} - \frac{1}{2}\pi\right)r_{d}^{2}}{\pi r_{d}} = \left(\frac{2\sqrt{3}}{\pi} - \frac{1}{2}\right)r_{d} = \left(\frac{2\sqrt{3}}{\pi} - \frac{1}{2}\right)\left(\frac{\gamma}{\Delta p}\right)$$

$$\approx 0.603 \frac{\gamma}{\Delta p}$$
(3.8)

As we can see, an increase in pressure over the layer of micelles Δp will mean more deformation and a subsequent reduction in the interstitial pore size r_h . At some moment, these pores will have a size similar to the hydrodynamic radius of the permeating proteins. Size exclusion will then occur. The simplest model describing size exclusion is Ferry's

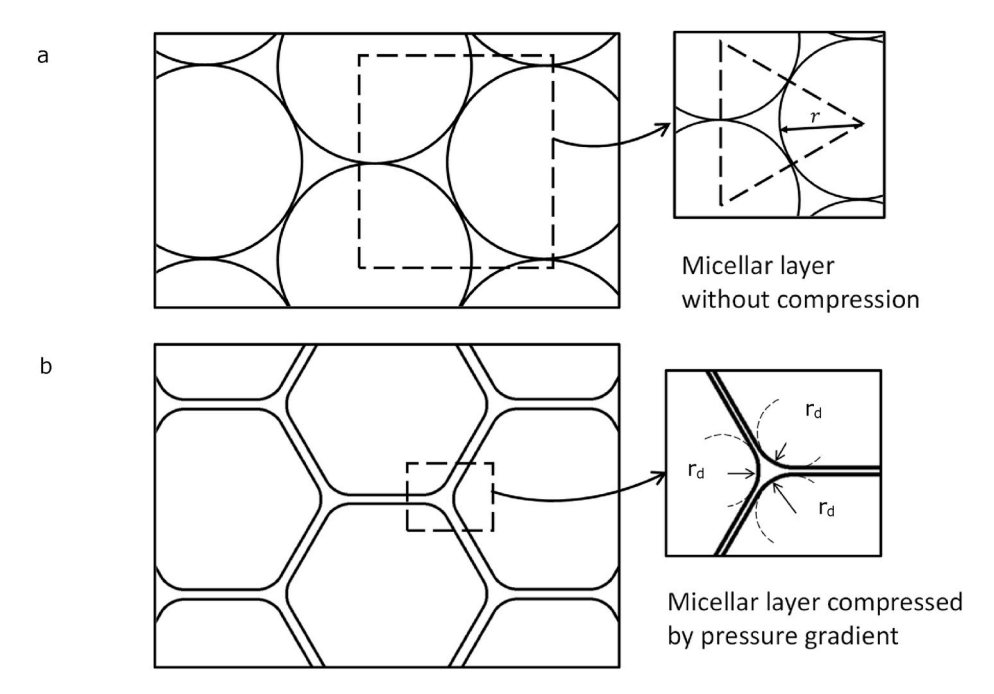


Fig. 2. (a)Depiction of a micellar layer without any compression. The interstitial pore size between the spheres is determined by the micellar size. The insert shows the geometry of the interstitial pore and the relevance of the micellar radius. (b): Depiction of a micellar layer that is compressed by the pressure gradient resulting from the flow rate of solvent through the membrane. The micelles are now compressed and compacted and assume a hexagonal shape. The geometry of the interstitial pores is determined by the radius of curvature of the micellar walls of the pores.

equation [43]; [39,44,45]:

$$\frac{C_m}{C_b} = \left(1 - \frac{r_s}{r_h}\right)^2 \tag{3.9}$$

As mentioned before the membrane pores give rise to some size exclusion. We can measure this exclusion during filtration when the transmembrane pressure is below critical transmembrane pressure using equation (3.2) (situation at which the fully developed concentration polarization layer is not yet fully developed or present on the membrane). When the increase in transmembrane pressure reaches and surpasses critical transmembrane pressure, the concentration polarization layer becomes fully developed and compressed. At this juncture, we then have two layers in series that both give rise to size exclusion. The

first is the membrane, as discussed; the second compressed micellar layer.

If we combine the effect of both the fully developed compressed concentration polarization layer (the very first layer next to the membrane) and the membrane, we get the total transmission (T):

$$T = \frac{C_m}{C_b} \times \frac{C_p}{C_m} = T_m \times T_r = \left(1 - \frac{r_s}{r_h}\right)^2 T_r = \left(1 - \frac{r_s \Delta p}{0.603 \, \gamma}\right)^2 T_r \tag{3.10}$$

 $T = C_p/C_b$ which is equal one minus the overall retention (T = 1 - R). This is illustrated in Fig. 3a.

After establishing the relevant equations necessary to estimate transmission of serum protein, we further proceeded to develop equa-

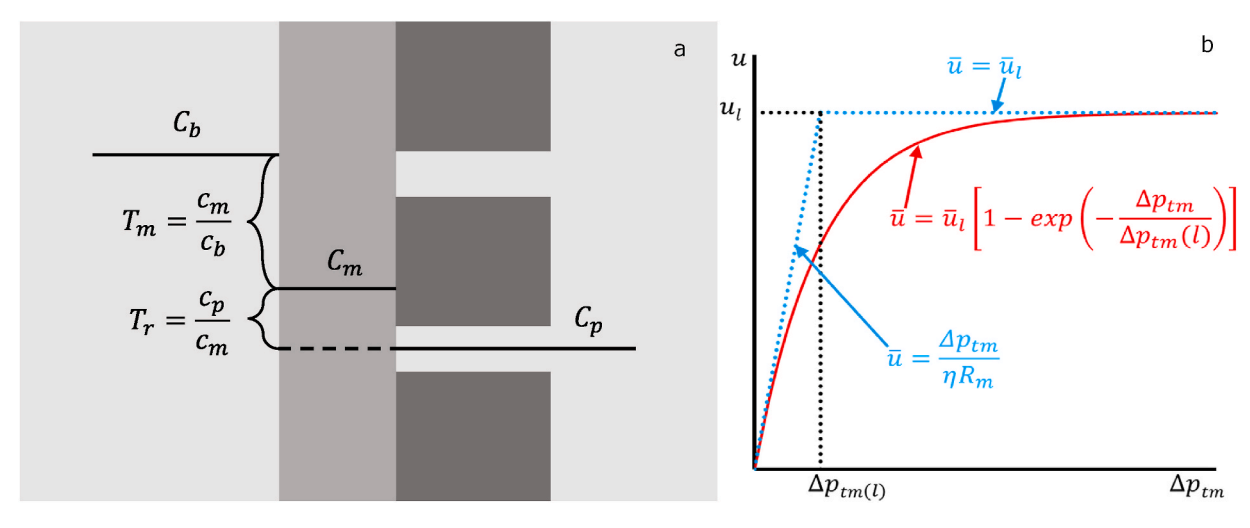


Fig. 3. (a) The total transmission and retention (R = 1 - T) is determined by two layers in sequence, the layer of compressed micelles just on top of the membrane, and the membrane pores. The total transmission is the product of both. (b) The figure above shows the transmembrane flux (blue) results obtained by the model and the equation used. The equation (red) uses the limiting transmembrane pressure and flux values obtained using equation (3.14) to further estimate and describe all the flux regimes as observed during experiments (red curve line). (For interpretation of the references to colour in this figure legend, the reader is referred to the Web version of this article.)

tions required for modelling the filtration kinetics versus the transmembrane pressure. A fully developed concentration polarization layer is only present when the volume fraction of the casein micelles on the membrane surface exceeds the $\varepsilon_{\rm rcp.}$ Before this, the casein dispersion is still fluid and will be swept away from the membrane due to crossflow. Therefore, up to a certain critical transmembrane flux, the size of the not fully developed concentration polarization layer will be minimal with large interstitial pores hence not effecting any retention of the dissolved proteins. Since ε in the concentration polarization layer is exceedingly high, the resulting hydraulic resistance in this not fully developed concentration polarization layer is negligible. Therefore, we can calculate the transmembrane flux with equation (3.11).

$$\overline{u} = \frac{\Delta p_{mn}}{\eta R_m} \tag{3.11}$$

The transmembrane flux calculated by equation (3.11) indicates the region where a linear relationship between flux and transmembrane pressure exists. Above this region, limiting transmembrane flux region exists and can be calculated using equation (3.13) [46]; [47].

$$\frac{\phi_m}{\phi_b} = \exp\left(\frac{\overline{u}_l}{k_{cp}}\right) \tag{3.12}$$

$$\overline{u}_l = k_{cp} \ln \left(\frac{1 - \epsilon_{rcp}}{\phi_b} \right) \tag{3.13}$$

As soon as $\phi_m=1-\epsilon_{rcp}=0.64$, the casein micelles on the membrane surface form a fully developed concentration polarization layer resulting in added resistance [48]. This implies that from this moment the steady-state transmembrane flux is determined by the (hydrodynamic) diffusion of casein micelles from the surface of the membrane to the bulk and the local size of the interstitial pores. Substituting $\phi_m=1-\epsilon_{rcp}=0.64$ in equation (3.12) results in equation (3.13).

Equation (3.14) predicts the limiting transmembrane flux regime using guess values of convective mass transfer coefficient (Table 2). The lines calculated with equations (3.11) and (3.13) cross each other at the limiting transmembrane pressure ($\Delta p_{tm~(1)}$). At pressures below $\Delta p_{tm~(1)}$ equation (3.11) is valid, while above $\Delta p_{tm~(1)}$ the transmembrane flux is equal to the limiting transmembrane flux (equation (3.13)). To further describe all flux regions as seen during experiments, equation (3.14) is used, which utilizes the values of limiting flux and transmembrane pressures from equation (3.13) [19,49].

$$\overline{u} = \overline{u}_l \left[1 - exp \left(-\frac{\Delta p_{m}}{\Delta p_{lm (l)}} \right) \right]$$
(3.14)

To use equations (3.10), (3.11) and (3.13), and 3.14, several

parameters are needed. Most parameters are obtained through experiments or from literature, while the $k_{\rm cp}$ of the micelles to the bulk, and the apparent γ of the micelles depend on the conditions and are found by comparing the model results with experimental results over a range of values in EXCEL.

There are two parameters that determine the retention of the soluble proteins which are interfacial tension, casein micelle size, and the random packing interstitial void fraction. However, the effect of a different value of $\epsilon_{\rm rcp}$ is not very large, and its effects can be absorbed in the adjustment of the interfacial tension, so we end up with only one adjustable parameter.

4. Results and discussion

4.1. Mode of pressure adjustment on flux and milk protein separation

To determine the irreversibility of deposits of casein on flux and transmission of proteins during filtration, an experiment was done by stepwise increasing followed by stepwise decreasing of the transmembrane pressure. The transmembrane pressure was adjusted in both stepwise increasing and stepwise decreasing sequences using five specific transmembrane pressure points: 0.3, 0.6, 1, 2, and 3 bar. Fig. 4 (left) shows that there was only an insignificant difference in flux between stepwise increase and stepwise decrease in transmembrane pressure. The transmembrane flux is dependent on the transmembrane pressure before reaching the limiting flux after which the transmembrane flux is only dependent on the hydrodynamic back-diffusion of the accumulating components, hence the constant flux regime. The estimated limiting transmembrane pressure is around 0.5 bar, while the obtained flux at 1 bar was 8.3 and 7.8 L m⁻² h⁻¹ during stepwise increase and decrease in transmembrane pressure, respectively. The difference observed was less than 10 %, after staying for a significant operation time deep in the constant flux regime (at up to 3 bars). The difference is observed after 45 min of stabilization, which allowed the relaxation of the concentration polarization layer that is formed during stepwise increase in transmembrane pressure. This demonstrates that the deposited micellar layer that is compressed onto the membrane due to the increase in transmembrane pressure is reversible at these temperatures.

The effect of the deposited casein micelles on the transmission of proteins is shown in Fig. 4 (right). Firstly, we can observe that the transmission of all proteins is reduced by the increase in transmembrane pressure. The caseins are mostly retained, with only 6 % being retained at low pressures, reducing to around 1 % at higher pressures. This indicates that the casein micelles are indeed retained, and that they remain stable, even at higher pressures, i.e., there is no significant solubilization of casein monomers at higher pressures. The whey proteins

Table 2 Modelling parameters both known and fitted parameters for flux and retention. Known parameters include casein micelle fraction, average casein micelle size, hydrodynamic sizes of β -lg, α -la, IgM and the random packing interstitial void ratio.

	Parameters for the flux		Parameters for the retention			
Known parameter	Feed volume fraction of casein micelles ^a Skim milk permeate viscosity	$\phi_b = 0.1$ $\eta (5^{\circ}C) = 2.2 \text{ mPa} \bullet s$ $\eta (10^{\circ}C) = 1.8 \text{ mPa.s}$ $\eta (15^{\circ}C) = 1.6 \text{ mPa} \bullet s$	Size of the casein micelles ^b Protein hydro-dynamic diameter	$D_b = 250 \text{ nm}$ β-lg = 3.5 nm α-la = 1.8 nm IgM = 36 nm		
	Membrane resistance	0.1 μ m (R_m) = 4 × 10 ¹² m^{-1} 0.2 μ m (R_m) = 8 × 10 ¹² m^{-1} 0.3 μ m (R_m) = 2 × 10 ¹² m^{-1}	Pressure	$\Delta p = range (0 - 3) bar$		
	Random packing interstitial void fraction ^d	$\epsilon_{rcp} = 0.36$	Tr factor	Transmission at 0 bar for all dissolved protein		
Fitted parameter	Mass transfer coefficient for casein micelles*	$k_{cp} = (0.9 - 2) \times 10^{-6} \frac{m}{s}$	Interfacial tension*	$\gamma = (1-10) \frac{mN}{m}$		

^{*}denotes the fitted parameters and a,b,c,d denotes the references.

^a [32]; [50].

^b [36]; [37,38]

c [33,35,51]

^d [52].

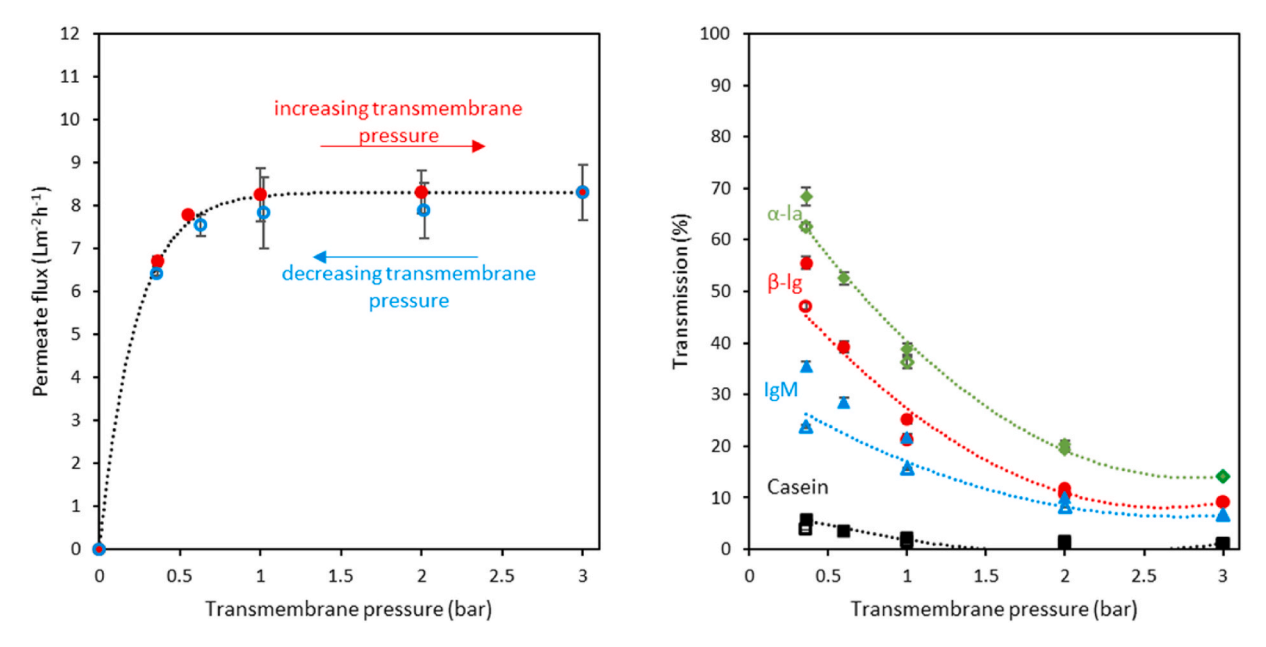


Fig. 4. (Left) The transmembrane flux in stepwise increase (red solid symbols) followed by stepwise decrease (blue open symbols) in TMP experiments using SYNDER Filtration spiral wound microfiltration membrane with pore size of $0.1~\mu m$ at a temperature of $10~^{\circ}$ C. Graph (right) shows the transmission of casein (black), β -lg (red), α -la (blue)and IgM (green) during stepwise increase (solid symbols) and stepwise decrease of transmembrane pressure (open symbols). The curves shown for both graphs are fitted trend lines to the experimental data. (For interpretation of the references to colour in this figure legend, the reader is referred to the Web version of this article.)

 α -la and β -lg show some retention at low pressures with 50–70 % transmission but are much more strongly retained at higher pressures: at 3 bar TMP. Their transmissions have been reduced to only 10–15 %.

Secondly, we observe full reversibility of the same proteins with stepwise decrease in transmembrane pressure. The casein transmission was 6 % at 0.3 bar during the ascending cycle which was reduced to 4 % during the descending cycle. For the whey proteins, after the pressure cycle, the β -lg transmission was reduced from 56 % to 47 %, and the α -la transmission reduced from 68 % to 64 % at the same conditions afore stated for casein. The small reductions in transmission can be attributed to some irreversible adsorption and fouling during compression in the

filtration process [53]. In essence, the measurements show that the process of serum protein retention is largely reversible. This demonstrates that for further experiments, following a stepwise increase in transmembrane pressure is an adequate strategy. Similar results were obtained by Hartinger et al. [28] who conducted skim milk fractionation experiments using PVDF spiral wound membranes at 10 and 50 °C.

4.2. Effect of temperature on transmembrane flux and milk proteins separation ${\it Separation}$

The effect of temperature was investigated at 5 °C, 10 °C, and 15 °C,

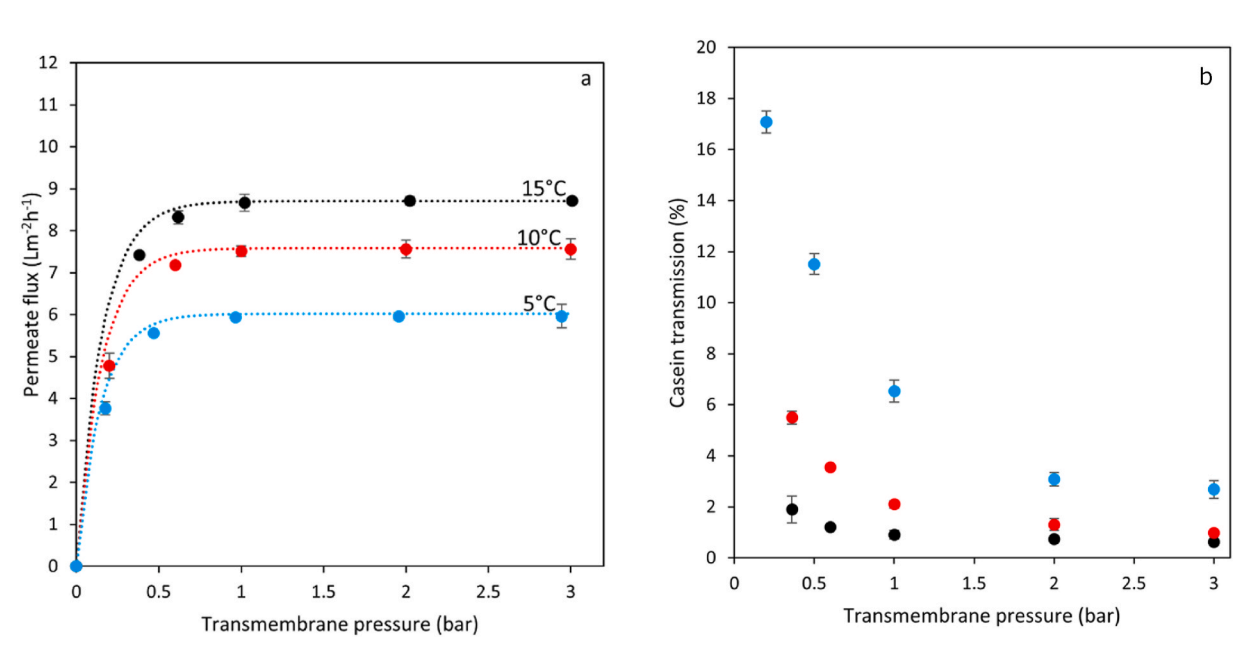


Fig. 5. (a) Results of transmembrane flux as obtained from the geometric model (...) and measured transmembrane flux (\bullet) using SYNDER Filtration spiral wound microfiltration membranes with pore size of 0.1 μ m at temperatures of 5 °C, 10 °C and 15 °C. (b) shows the transmission of casein using the same membrane at the same temperature conditions.

using PVDF spiral wound membranes with a nominal pore size of 0.1 μ m. The transmembrane flux at these different temperatures is shown in Fig. 5a. The limiting flux and transmembrane pressure were obtained using equations. The limiting transmembrane flux was found to be 5.5 L $m^{-2} h^{-1}$, 7.3 L $m^{-2} h^{-1}$ and 8.3 L $m^{-2} h^{-1}$ at 5 °C, 10 °C, 15 °C respectively with the corresponding limiting transmembrane pressures being 0.15 bar for all temperatures investigated. An increasing trend in transmembrane flux with an increase in temperature was observed even at these lower temperatures. The decrease in transmembrane flux at 5 $^{\circ}$ C is due to the increase in viscosity of the retentate which results in less turbulence on the membrane surface, hence a lower mass transfer coefficient k_{cp} . This then limits the transport of dissolved proteins through the membrane. Equal limiting transmembrane pressure indicates that the behavior and arrangement of the casein micelles on the membrane surface was similar for all the temperature conditions investigated. Exceptionally low limiting transmembrane pressure suggests that the formation of a fully developed concentration polarization layer happens early on and above it this layer has major impact on filtration. From the results of the model, the effect of temperature on viscosity and mass transfer was taken into account and a good fit was obtained as seen in Fig. 5a. Since temperature has an effect on the mass transfer, the following values at 5 $^{\circ}$ C, 10 $^{\circ}$ C, and 15 $^{\circ}$ C were fitted in to the model namely $9.07 \times 10^{-7} \text{ m s}^{-1}$, $1.1 \times 10^{-6} \text{ m s}^{-1}$, and $1.3 \times 10^{-6} \text{ m s}^{-1}$ respectively. The effect of change in mass transfer can be seen in figure A.1 in the appendix. It is observed that the mass transfer increases with the increase in temperature hence is attributed to the increase in transmembrane flux with increase in temperature. However, it should be noted that the membrane resistance was kept constant at 4×10^{12} m⁻¹.

We expect that also the transmission behavior will be temperature dependent since the apparent interfacial tension of the micelles will be temperature dependent. The calculated casein transmissions at transmembrane pressure of 1 bar were 6.5 %, 2.1 %, and 0.9 % at 5 $^{\circ}$ C, 10 $^{\circ}$ C, $15\,^{\circ}$ C, respectively, as shown in Fig. 5b. The difference in transmission is due to the progressive dissociation of β -casein from the micelles since it exists in monomeric state at temperatures of between 0 and 5 °C into the serum phase hence changing the micelle size. Since β-casein has high potential for hydrophobic interactions, decrease in temperature weakens this interaction [18] accounting for the strong increase in casein transmission at low temperatures. Our findings are in agreement with previous studies that also reported higher transmission of casein at lower operation temperatures. Some researchers reported casein transmission in the range of 0-20 % [54-56] for temperatures between 5 and 23 °C. In addition to permeate, the mass flux is used as a measure of filtration performance and could clearly show the differences between

the different filtration temperatures used figure A.3 in the appendix.

Within the applied temperatures, there is a slight difference in the transmission of beta lactoglobulin (β -lg) and alpha lactalbumin (α -la) observed as seen in Fig. 6, albeit not nearly as large as for the casein. The small reduction in transmission with higher temperatures, may be due to some changes in the properties of the micelles such as size, but may also be related to changes in the electrostatic and steric interactions between the different proteins, when permeating through the concentration polarization layer. Due to the dissociation of beta casein at for example 5 °C, this could have an impact on the micelles in the developed concentration polarization layer. Due to the loss of the beta casein the structure of the micelles is impacted and could further increase the porosity of the micelles hence explaining why transmission of β-lg is slightly increased. Before limiting transmembrane pressure, transmission is only hindered by the membrane since no stagnant concentration polarization layer has yet fully developed. After the formation of this stagnant layer, the interstitial pore size between the deformable casein micelles reduces due to the increase in the applied transmembrane pressure. The transmission of IgM, however, is similar in all the temperatures investigated. Since IgM is a relatively larger protein, slight changes of the properties of the micelles due to dissociation of the micelles have no significant effect on transmission. This layer then becomes the dominant sieving layer with the results shown in Fig. 6.

Table 3 shows the fitted apparent interfacial tension values of the casein micelles for β -lg, α -la and IgM transmission. All values were within the range of 1–2 mN m⁻¹ for the three temperature conditions and different pore sizes. The fact that the deformability of the casein micelles along the concentration polarization layer is uniform at each temperature condition agrees with the assumption in the model. This assumption is that the micelles are reversibly deformed, and that the deformability only depends on the thermodynamic state of the micelles, i.e., the temperature, if ionic strength, pH, and other parameters to remain the same. The fact that the apparent interfacial tension is lowest at 5 °C, agrees with the increasing hydration of casein at lower temperatures, which will lead to larger voluminosity and larger deformability under compression. The apparent molecular size of the permeating protein was fitted with the model. While for β -lg and α -la the values are quite close to their reported hydrodynamic size, the value for IgM is much smaller than expected, given that the molecule is approximately 900 kDa which is much larger than β -lg and α -la. One should however bear in mind that IgM is not spherical as assumed in the model, but an oblate spheroid with 3 diameters; two of them being equal at 37 nm and one diameter 6 nm [51]. The molecule could therefore permeate along its longest axis through the pores. Additionally, IgM consists of

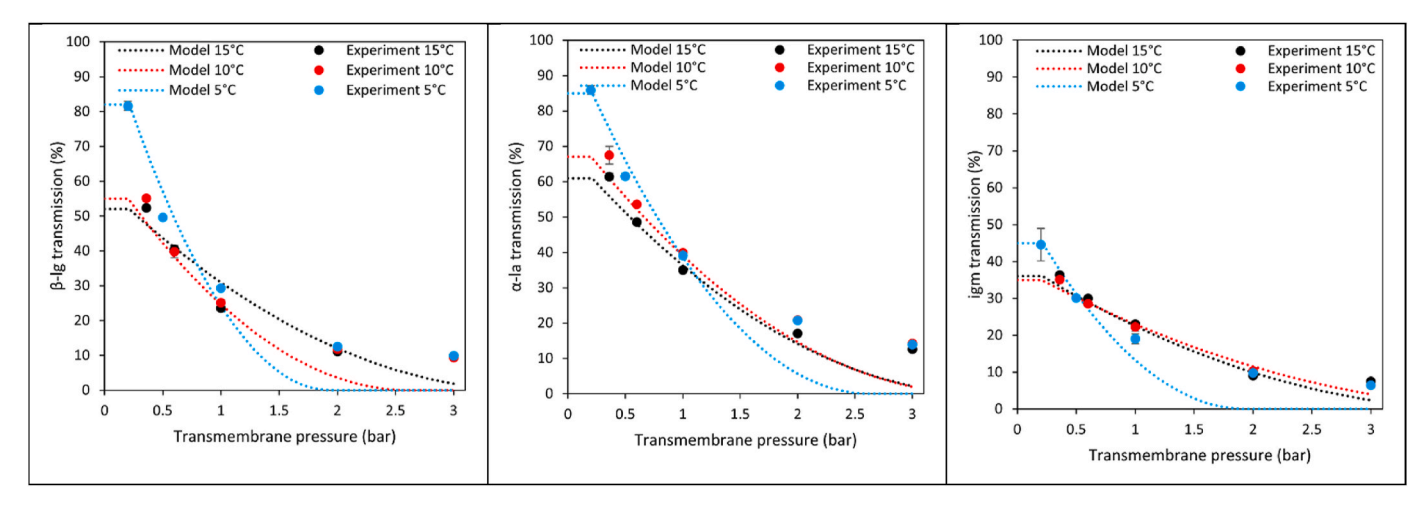


Fig. 6. The graphs show the experimental (dots) and modelling transmission data (dotted lines) for β -lg (left) α -la (middle) and IgM (right) respectively with respect to change in transmembrane pressure at 5 °C, 10 °C, and 15 °C. These experiments were carried out using SYNDER Filtration spiral wound microfiltration membrane with pore size of 0.1 μ m.

Table 3

Apparent micellar interfacial tension of casein micelles during filtration as function of the temperature and pore size. The fitted Tr factor and protein size for each condition are also listed.

	Casein micelle interfacial tension (mN. \mbox{m}^{-1})		Tr factor (transmission as a result of membrane pore exclusion)			Fitted protein size (nm)			Transmission R ²			
Condition	β-lg	α-la	IgM	β-lg	α-la	IgM	β-lg	α-la	IgM	β-lg	α-la	IgM
0.1 μm pore size (15 °C)	2	2	2	0.52	0.61	0.36	3.5	3.5	3.2	97.3	96.0	97.4
0.1 μm pore size (10 °C)	1.4	1.4	1.4	0.55	0.67	0.35	3.5	2.5	2	99.1	99.1	99.1
0.1 μm pore size (5 °C)	1	1	1	0.82	0.85	0.45	3.5	2.5	3.5	95.9	95.6	97.2
0.2 μm pore size	1.4	1.4	1.4	0.53	0.62	0.39	2.8	1.9	2	98.2	98.0	98.9
0.3 μm pore size	1.4	1.4	1.4	0.79	0.86	0.47	5	4	2.5	98.0	97.5	99.5

two identical antigen binding regions: an antigen binding region and a crystallizable region, linked together by a mobile hinge with no secondary structure [51]. This allows the protein to be highly flexible thus possessing the ability to pass even through the pores in between the deformed micelles. During filtration, assuming that IgM permeates along its longest of 6 nm, the flexibility of this molecule would also reduce the size further. Accounting for this flexibility in the model, the effective size of the IgM varied between 37 nm and 2 nm since the interfacial tension is constant as shown in Table 3. The differences in fit when using the largest IgM diameter of 37 nm, smallest diameter of 6 nm and 2 nm can be seen in figure A.2 in appendix. 37 nm reflects zero transmission at all the applied transmembrane pressures and it's only with the smallest diameter (2 nm) that we have transmission reflecting what we obtained during experiments.

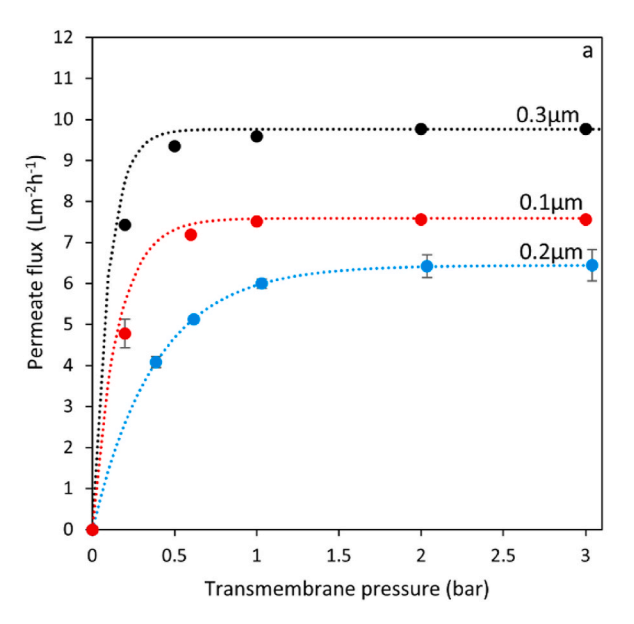
Fig. 6 shows that while the description of the data with our simple geometric model is adequate at pressures until 2 bar, the fit is considerably worse above this transmembrane pressure. We hypothesize that this could be because at these higher pressures the permeating proteins cannot be considered hard spheres anymore. Their flexibility there could account for higher transmission at transmembrane pressures above 2 bar with experiments but not with the model. Also, the shape of the pores is not cylindrical as seen in Fig. 2 thus allowing the non-spherical proteins to still permeate through this layer. Additionally, casein micelles are porous, and this could allow some soluble proteins to pass through even when the pores between the micelles are diminished. However, at these low transmissions, one may expect that other interactions than just size become important as well.

From Table 3, we observe that at higher temperature the interfacial

tension is higher as compared to lower temperature and there is no effect of membrane pore size on the interfacial tension. Interfacial tension of casein micelles is dependent on the temperature since increase and decrease in temperature can affect several factors such as micelle structure, molecular motion, solubility, and critical micelle concentration. When these factors are changed flexibility, solubility, and the arrangement of the micelles are altered resulting in either an increase or decrease in interfacial tension. Further, the fitted protein sizes were varied to obtain the best fit with the experimental data. The change we observe with change in temperature could be due to folding or unfolding of proteins but also dependent on size of the interstitial pore and what size it can accommodate. The fitted protein size is also dependent on interstitial pore size since the bigger the pore the higher the transmission due to the membrane. This then means that the size of the molecule passing through is higher based on Equation (3.10). The Tr factor represents the exclusion caused by the membrane itself while the fitted protein size is compared to the sizes of the proteins reported in literature. B-lg is reported in literature to be 3.5-4.2 nm in sizes [33,35,51], α -la is 1.-2.5 nm in size [33,51] and IgM is 25–37 nm in size [51].

4.3. Effect of pore size on transmembrane flux and protein transmission

PVDF membranes with different pore sizes ranging between 0.1 and 0.3 μm were then used. Fig. 7 shows that the membrane with pore size 0.3 μm had the highest transmembrane flux and the membrane with 0.2 μm pore size having the lowest transmembrane flux. A higher flux is observed when the pore size is reduced from 0.2 μm to 0.1 μm . While part of this may stem from differences in membrane porosity, other



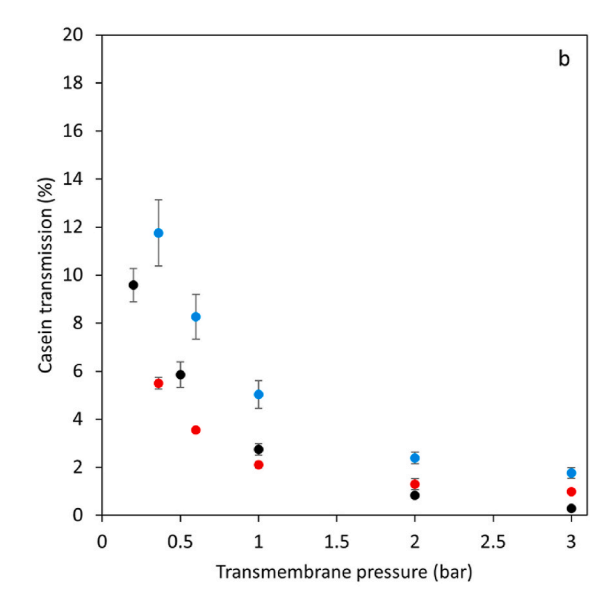


Fig. 7. (a) Results of transmembrane flux as obtained from the model (... ...) and measured transmembrane flux (\bullet) using spiral wound microfiltration membranes with pore size of 0.1 μ m (red), 0.2 μ m (blue) and 0.3 μ m (black) at temperatures of 10 °C. (b) shows the transmission of casein using the same membrane at different pore sizes. (For interpretation of the references to colour in this figure legend, the reader is referred to the Web version of this article.)

factors could play a role. These factors include the pore size distribution and that the average size of micelles is equal to $0.2~\mu m$. The effect of reduced transmembrane flux when the membrane pores size is $0.2\ \mu m$ has also been investigated by other researchers showing similar behavior. Heidebrecht et al. used ceramic membranes of $0.14~\mu m,\,0.2$ μm, 0.45 μm and 0.8 μm pore size with rather similar porosities and observed a lower flux with their 0.2 µm pore size membrane as compared to the others [34]. In addition to what Heidebrecht observed, it is our opinion that above the critical flux point, the flux is determined by the hydrodynamic back-diffusion of the micelles from the membrane surface. This can further be seen from the change in the mass transfer coefficients at different membrane pore sizes. The mass transfer coefficient was fitted and the following were used 1.46×10^{-6} m.s⁻¹, $9.63 \times 10^{-7} \text{ m.s}^{-1}$, and $1.1 \times 10^{-6} \text{ m.s}^{-1}$ for the 0.3 μ m, 0.2 μ m and 0.1 μm membranes respectively. These differences are related to slight differences in the exact module geometry. The difference in transmembrane fluxes is also attributed to difference in the membrane resistance. 0.2 µm pore size membrane had the highest membrane resistance with 0.3 µm membrane having the lowest membrane resistance. The limiting transmembrane pressures are 0.1, 0.28, and 0.15 bar for the 0.3 μ m, 0.2 μ m and 0.1 μ m membranes, respectively.

As expected, the membrane with 0.1 μm pore size had the lowest transmission for casein as compared to the other two membranes (Fig. 7). This nominal pore size is smaller than the average size of casein micelles and hence good retention is observed. The transmission of casein observed may be due to the smaller micelles (below 100 nm) passing through the membrane, and to permeation through the few larger pores in the membrane, as the membrane will have a distribution in pore sizes. The 0.2 μm and 0.3 μm membranes show higher transmissions due to their larger pore sizes which will allow slightly larger micelles to pass through, especially through their largest pores.

For the whey proteins (Fig. 8), we see similar behavior as reported in Fig. 6. However, the difference in transmission between different membranes is relatively small for each type of protein (α -la, β -lg and IgM). This can be understood based on the model. While at low transmembrane pressures the transmission is mostly determined by the intrinsic exclusion by the membrane pores, the transmission of dissolved proteins at higher transmembrane pressures is mostly determined by the layer of compressed casein micelles. The differences that are still there can be explained by the pressure drops within the membranes since all the membranes have different resistances (Table 2). This pressure drop is different for each type of membrane and hence the degree of compression differences over the stagnant micellar concentration polarization layer.

As in Fig. 6, we can observe from Fig. 8 that the fit of the model from the lowest transmembrane pressure to approximately 1 bar is near perfect, while at 2 bars and higher, the model estimates a lower transmission than what was measured during experiments. The explanation is the same as before, in that at higher transmembrane pressures the intermicellar pores become quite small and the exact shapes and deformability of the permeating components become important.

5. Conclusion

We present flux and transmission measurements of the individual proteins in crossflow microfiltration of skim milk. Micellar caseins are almost completely retained, while the retention of the whey proteins is relatively low at low transmembrane pressures but increases rapidly with larger transmembrane pressures. We explain this by assuming a two-layer model. The first layer is the membrane itself and depending on the severity of pore blocking by casein micelles the transmission of whey proteins at transmembrane pressure lower than limiting transmembrane pressure is determined. Upon reaching the limiting transmembrane pressure, a second layer of compressed casein micelles forms on the membrane. The interstitial pores between these compressed micelles become progressively smaller at higher transmembrane pressures due stronger compression of the micelles onto each other. Temperature dependence showed that the deformability of the casein micelles increases with lower temperatures, as expected based on hydration. Membranes having larger pores (from 0.1 to 0.3 μm nominal pore sizes) showed no significant differences between the transmission of whey proteins between the three membranes, which is in accordance with the proposed mechanism.

A simple geometric model describing the compression of the casein micelles could quantitatively model the retention behavior at most pressures, except at higher transmembrane pressures. At higher transmembrane pressures, the assumptions in our relatively simple model break down, and the exact shapes of the permeating molecules become important. This simple model has helped to show that indeed the casein micelles are reversibly compressed onto the membrane, and it becomes a dynamic membrane that dominates the retention of the whey proteins. Optimization of the separation between caseins and whey proteins therefore should take into account this strong interaction between the different proteins in the system. The simplicity of the presented geometric model shows that this is possible and does not have to be complex. We recommend inclusion of the permeability of the case in layer as a function of the local interstitial void volume and the compressibility of β -lg, α -la, and IgM so as to describe in depth the transmission of these proteins especially in the high pressure regimes above 1 bar.

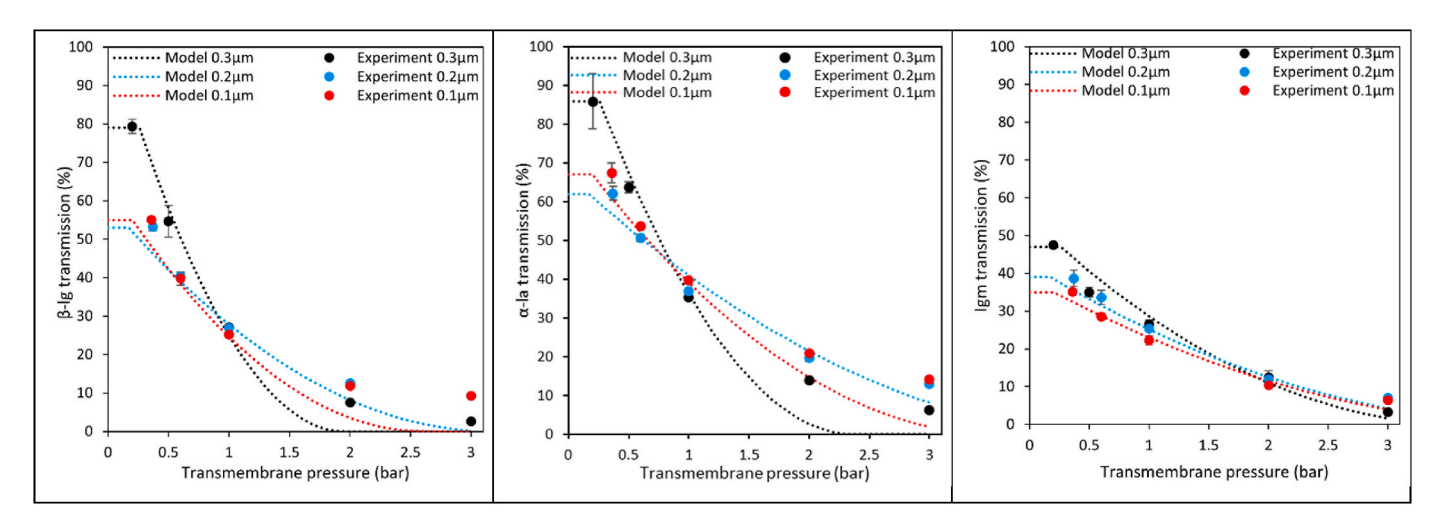


Fig. 8. The experimental (points) and modelling transmission data (dotted lines) for β -lg (left), α -la (middle) and IgM (right) respectively with respect to change in transmembrane pressure using 0.1 μm pore size, 0.2 μm and 0.3 μm pore size membranes at 10 °C are shown.

CRediT authorship contribution statement

Hilda Lucy Nyambura: Writing – review & editing, Writing – original draft, Visualization, Methodology, Investigation, Formal analysis, Conceptualization. Anja E.M. Janssen: Writing – review & editing, Supervision, Conceptualization. Albert van der Padt: Writing – review & editing, Supervision, Conceptualization. Remko M. Boom: Writing – review & editing, Supervision, Conceptualization.

Declaration of competing interest

The authors declare that they have no known competing financial interests or personal relationships that could have appeared to influence

the work reported in this paper.

Acknowledgements

This publication is part of an Institute for Sustainable Process Technology (ISPT) project, i.e., Novel Process Routes (Reduction of Energy use by Novel process routes for food). Partners in this project are Cosun, DSM, FrieslandCampina, Pentair, NIZO, Wageningen University & Research, TU Delft and ISPT. This project is co-funded by TKI-Energy with the supplementary grant "TKI- Toeslag" for Topconsortia for Knowledge and Innovation (TKI's) of the Ministry of Economic Affairs and Climate Policy.

Nomenclature

Α	Area of Interstitial pore (m ²)	r_p	Membrane pore diameter (m)
A_C	Area of the circle	r_s	Serum protein size (m)
A_T	Cross-sectional area of the triangle (m ²)	T	Total transmission as a result of exclusion of the compressed layer and the membrane (%)
C_b	Bulk concentration (g/l)	T_m	Transmission as a result of exclusion of the compressed layer (%)
C_m	Concentration in the very first layer of the compressed casein micelle layer next to the membrane (g/l)	T_r	Transmission as a result of exclusion of the membrane (%)
C_p	Permeate concentration (g/l)	ε	Void fraction
C_r	Retentate concentration (g/l)	$\varepsilon_{\rm rcp}$	Maximum random packing
d_{cas}	Average diameter of the casein micelles (m)	η	Viscosity of the permeate (Pa. s)
d_h	Hydraulic diameter of the interstitial pore (m)	Φ	Exclusion factor
k_{cp}	Convective mass transfer coefficient of casein (ms ⁻¹)	ϕ_b	Volume fraction of casein in the bulk
\boldsymbol{P}	Wetted perimeter of the pore (m)	ϕ_m	Volume fraction of casein at the membrane
P_f	Feed pressure (Pa or bar)	Δp	Pressure gradient over the casein micelle layer (Pa)
P_r	Retentate pressure (Pa or bar)	Δp_{tm}	Transmembrane pressure (Pa or bar)
P_p	Permeate pressure (Pa or bar)	$\Delta p_{tm~(l)}$	Limiting transmembrane pressure (Pa)
R	Total rejection of the dissolved protein (%)	\overline{u}	Transmembrane flux (Lm ⁻² h ⁻¹)
r	Radius of the sphere (m)	$\overline{u_l}$	Limiting transmembrane flux (Lm ⁻² h ⁻¹)
r_d	Radius of curvature of the micellar walls of the interstitial pore (m)	γ	Interfacial tension (mN/m)
r_h	Hydraulic radius of the interstitial pore (m)		
R_m	Membrane resistance (m ⁻¹)		

Appendices.

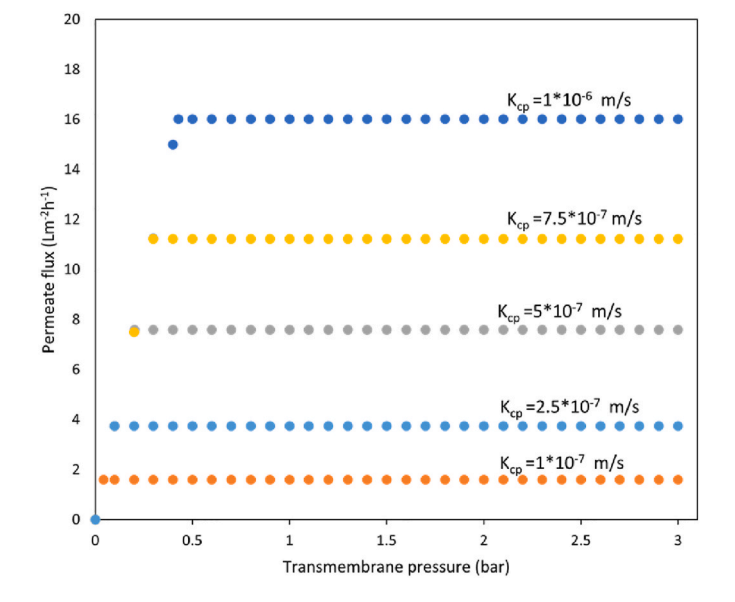


Fig. A.1. Resulting transmembrane flux with changing mass transfer coefficient.

This shows the effect of change in casein mass transfer coefficient on the transmembrane flux. The lower the mass transfer, the higher the transmembrane flux since the resistance is reduced.

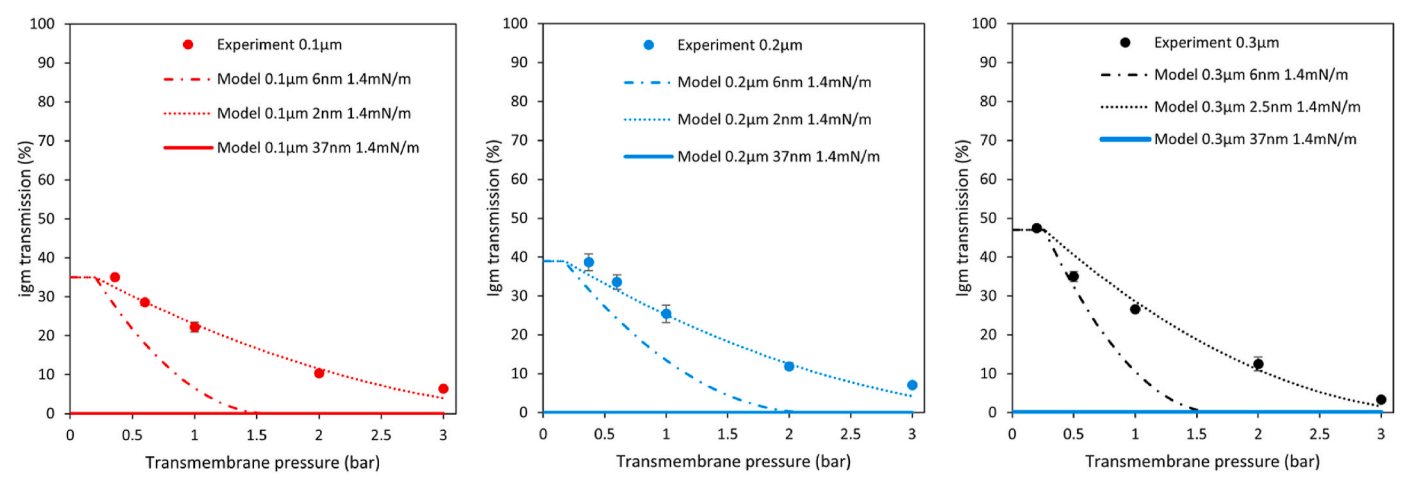


Fig. A.2. This figure shows the fit of the model to the experimental results for IgM with sizes (6 and 37 nm) reported in literature and 2 and 2.5 nm (approximation) at the same interfacial tension.

With different pore sizes of the membrane, there was no transmission of IgM when the diameter is kept at 37 nm. When we varied the diameter to use the third diameter of 6 nm since it is an oblate spheroid then significant transmission was observed but still there was no fit. We further reduced the diameter to approximately 2 nm and we obtained a better fit to the experimental data.

Mass flux is a measure that can aid in further evaluating the performance of different operation conditions since there is no significant difference observed with transmission of whey proteins. The mass fluxes of β -lg and α -la and IgM were calculated, and results shown below. For β -lg, α -la, and IgM, increasing temperature results in an increase in the amount of protein that is transmitted through the membrane. This is due to the decrease in viscosity and density of the feed used with increasing temperature. This facilitates further reduction in the size of the concentration polarization layer reducing the resistance of the protein transmission.

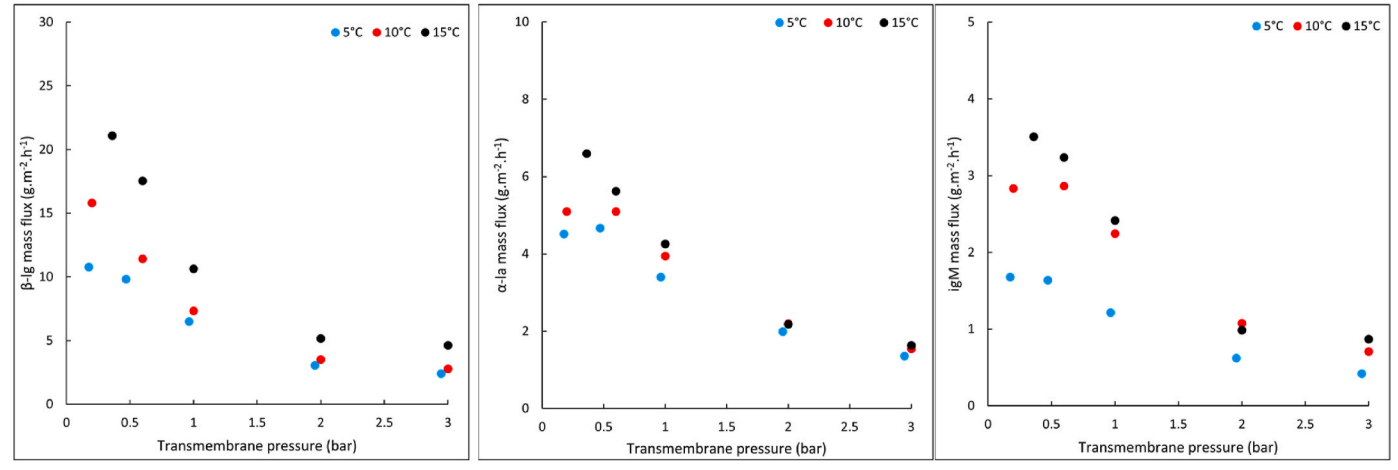


Fig. A.3. Mass flux calculated from the experimental data with respect to change in transmembrane pressure for SYNDER Filtration spiral wound microfiltration membrane with pore size of 0.1 μ m at temperatures of 5 °C 10 °C and 15 °C.

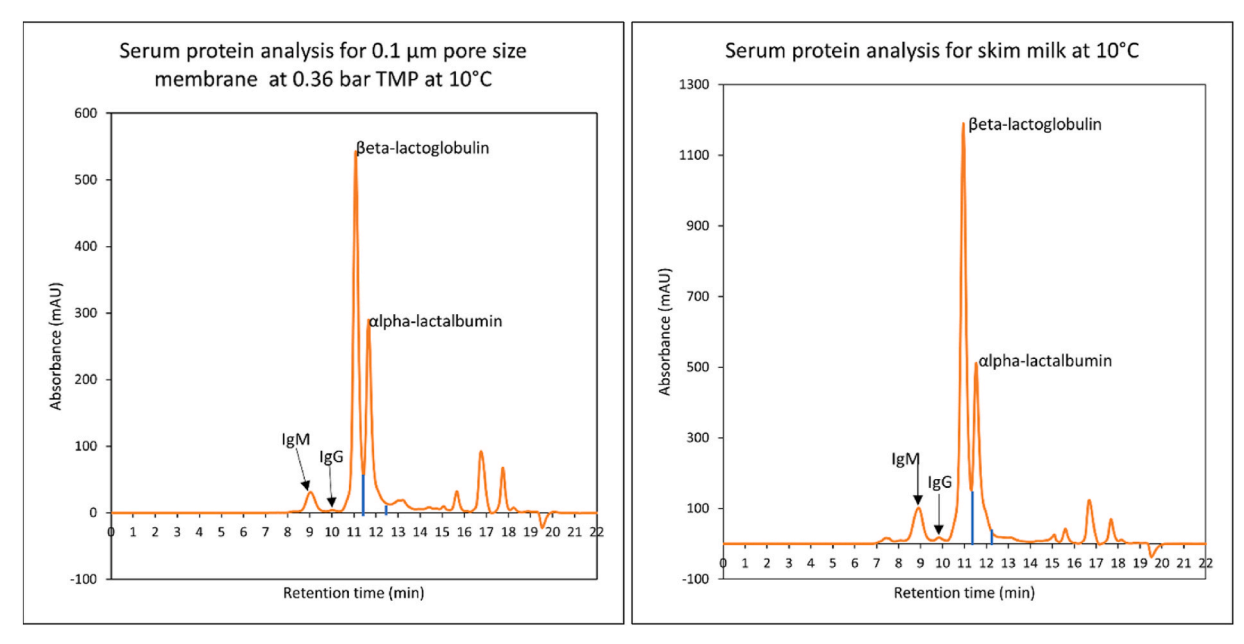


Fig. A.4. Graph on the left shows the chromatogram for a permeate sample that was analyzed to ascertain the serum protein concentration. This permeate sample was obtained using 0.1 μ m pore size membrane at 0.36 bar transmembrane pressure at 10 °C. Graph on the right shows the same for a sample of skim milk that was analyzed to ascertain the concentration of serum protein in skim milk.

The area under each peak is then calculated by multiplying the peak width in minutes by the peak height in absorbance. With that area, a calibration curve such as the one given by figure A.5, is then used to calculate the concentration of each serum protein and casein.

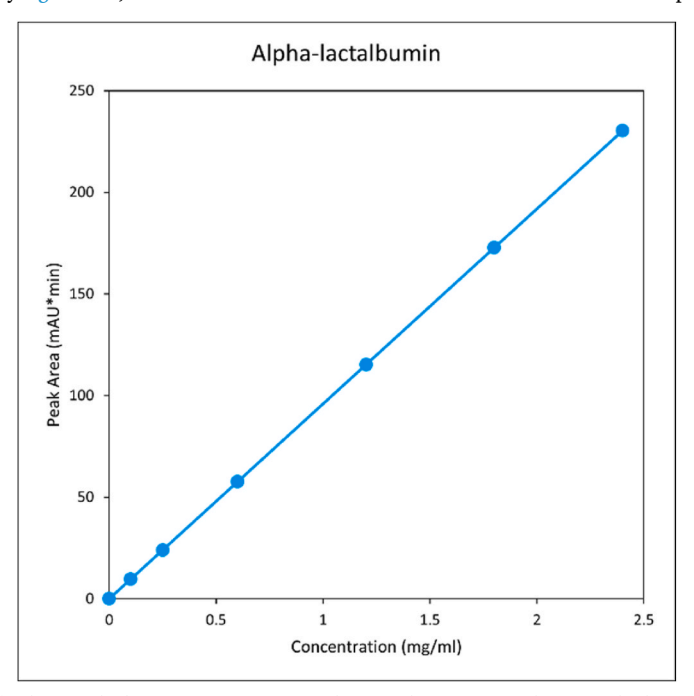


Fig. A.5. Standard calibration curve of α -la to calculate its concentration (three replications are shown with the corresponding standard deviation but are exceedingly small hence not visible).

Data availability

Data will be made available on request.

References

[1] H.N. Blais, K. Schroën, J.T. Tobin, A review of multistage membrane filtration approaches for enhanced efficiency during concentration and fractionation of milk and whey, Int. J. Dairy Technol. 75 (4) (2022) 749–760, https://doi.org/10.1111/ 1471-0307.12884.

- [2] N.A. Burd, Y. Yang, D.R. Moore, J.E. Tang, M.A. Tarnopolsky, S.M. Phillips, Short Communication Greater stimulation of myofibrillar protein synthesis with ingestion of whey protein isolate v . micellar casein at rest and after resistance exercise in elderly men, Br. J. Nutr. (2012) 958–962, https://doi.org/10.1017/ S0007114511006271.
- [3] M.C. Devries, S.M. Phillips, Supplemental protein in support of muscle mass and health: advantage whey, J. Food Sci. 80 (S1) (2015), https://doi.org/10.1111/ 1750-3841.12802.
- [4] Y.C. Luiking, N.E.P. Deutz, R.G. Memelink, S. Verlaan, R.R. Wolfe, Postprandial muscle protein synthesis is higher after a high whey protein, leucine-enriched supplement than after a dairy-like product in healthy older people: a randomized

- controlled trial, Nutr. J. 13 (9) (2014) 1-14, https://doi.org/10.1186/1475-2891-
- [5] R. Schopf, F. Desch, R. Schmitz, D. Arar, U. Kulozik, Effect of flow channel number in multi-channel tubular ceramic microfiltration membranes on flux and small protein transmission in milk protein fractionation, J. Membr. Sci. 644 (November 2021) (2022) 1–9, https://doi.org/10.1016/j.memsci.2021.120153.
- [6] G. Brans, C.G.P.H. Schroën, R.G.M. Van Der Sman, R.M. Boom, Membrane fractionation of milk: state of the art and challenges, J. Membr. Sci. 243 (1–2) (2004) 263–272, https://doi.org/10.1016/j.memsci.2004.06.029.
- [7] M. Loginov, F. Doudiès, N. Hengl, M. Karrouch, N. Leconte, F. Garnier-Lambrouin, J. Pérez, F. Pignon, G. Gésan-Guiziou, On the reversibility of membrane fouling by deposits produced during crossflow ultrafiltration of casein micelle suspensions, J. Membr. Sci. 630 (October 2020) (2021), https://doi.org/10.1016/j. memsci.2021.119289.
- [8] H. Buzás, G. Szafner, M. Krassóy, A. Wiedmann, A.J. Kovács, Effect of pore size and temperature on the behaviour of alpha-lactalbumin and the A and B genetic variants of beta-lactoglobulin during protein fractionation microfiltration, Food Hydrocoll. 160 (July 2024) (2025), https://doi.org/10.1016/j. foodhyd.2024.110759.
- [9] F. Doudiès, M. Loginov, N. Hengl, M. Karrouch, N. Leconte, F. Garnier-Lambrouin, J. Pérez, F. Pignon, G. Gésan-Guiziou, Build-up and relaxation of membrane fouling deposits produced during crossflow ultrafiltration of casein micelle dispersions at 12 °C and 42 °C probed by in situ SAXS, J. Membr. Sci. 618 (July 2020) (2021), https://doi.org/10.1016/j.memsci.2020.118700.
- [10] E.I. Melnikova, E.B. Stanislavskaya, E.V. Bogdanova, Technological parameters of microfiltration in the production of micellar casein concentrate, Curr. Nutr. Food Sci. 20 (4) (2023) 520–528, https://doi.org/10.2174/ 0115734013266503230919071431.
- [11] K. Karasu, N. Glennon, N.D. Lawrence, G.W. Stevens, A.J. O'connor, A.R. Barber, S. Yoshikawa, S.E. Kentish, A comparison between ceramic and polymeric membrane systems for casein concentrate manufacture, Int. J. Dairy Technol. 63 (2) (2010) 284–289, https://doi.org/10.1111/j.1471-0307.2010.00582.x.
- [12] N.D. Lawrence, S.E. Kentish, A.J. O'Connor, A.R. Barber, G.W. Stevens, Microfiltration of skim milk using polymeric membranes for casein concentrate manufacture, Separ. Purif. Technol. 60 (3) (2008) 237–244, https://doi.org/ 10.1016/j.seppur.2007.08.016.
- [13] F. Tokay, S. Bağdat, A novel and simple approach to element fractionation analysis: single step fractionation of milk, Food Chem. 379 (July 2021) (2022), https://doi. org/10.1016/i.foodchem.2022.132162.
- [14] S.L. Beckman, J. Zulewska, M. Newbold, D.M. Barbano, Production efficiency of micellar casein concentrate using polymeric spiral-wound microfiltration membranes, J. Dairy Sci. 93 (10) (2010) 4506–4517, https://doi.org/10.3168/ ids.2010-3261.
- [15] S.V. Crowley, V. Caldeo, N.A. McCarthy, M.A. Fenelon, A.L. Kelly, J.A. O'Mahony, Processing and protein-fractionation characteristics of different polymeric membranes during filtration of skim milk at refrigeration temperatures, Int. Dairy J. 48 (2015) 23–30, https://doi.org/10.1016/j.idairyj.2015.01.005.
- [16] T.C. France, F. Bot, A.L. Kelly, S.V. Crowley, J.A. O'Mahony, The influence of temperature on filtration performance and fouling during cold microfiltration of skim milk, Separ. Purif. Technol. 262 (December 2020) (2021) 118256, https:// doi.org/10.1016/j.seppur.2020.118256.
- [17] J.M. van der Schaaf, D.A. Goulding, C. Fuerer, J. O'Regan, J.A. O'Mahony, A. L. Kelly, A novel approach to isolation of β-casein from micellar casein concentrate by cold microfiltration combined with chymosin treatment, Int. Dairy J. 148 (2024) 105796, https://doi.org/10.1016/j.idairyj.2023.105796.
- [18] B. Holland, M. Corredig, M. Alexander, Gelation of casein micelles in β-casein reduced milk prepared using membrane filtration, Food Res. Int. 44 (3) (2011) 667–671, https://doi.org/10.1016/j.foodres.2010.11.032.
- [19] C. Astudillo-Castro, A. Cordova, V. Oyanedel-Craver, C. Soto-Maldonado, P. Valencia, P. Henriquez, R. Jimenez-Flores, Prediction of the limiting flux and its correlation with the Reynolds number during the microfiltration of skim milk using an improved model, Foods 9 (11) (2020) 1621, https://doi.org/10.3390/ foods9111621.
- [20] G. Samuelsson, I.H. Huisman, G. Trägårdh, M. Paulsson, Predicting limiting flux of skim milk in crossflow microfiltration, J. Membr. Sci. 129 (2) (1997) 277–281, https://doi.org/10.1016/S0376-7388(97)00013-6.
- [21] P. Bacchin, M. Meireles, P. Aimar, Modelling of filtration: from the polarised layer to deposit formation and compaction, Desalination 145 (2002) 139–146, https:// doi.org/10.1016/S0011-9164(02)00399-5.
- [22] N. Schork, S. Schuhmann, H. Nirschl, G. Guthausen, In situ measurement of deposit layer formation during skim milk filtration by MRI, Magn. Reson. Chem. 57 (9) (2019) 738–748, https://doi.org/10.1002/mrc.4826.
- [23] R. Gebhardt, Effect of filtration forces on the structure of casein micelles, J. Appl. Crystallogr. 47 (2014) 29–34, https://doi.org/10.1107/S1600576713029841.
- [24] A. Bouchoux, P. Qu, P. Bacchin, A general approach for predicting the filtration of soft and permeable colloids: the milk example, Am. Chem. Soc. 30 (1) (2013) 22–34, https://doi.org/10.1021/la402865p.
- [25] W.S. Opong, A.L. Zydney, Diffusive and convestive protein transport through asymmetric membranes, AIChE J. 37 (10) (1991) 1497–1510, https://doi.org/ 10.1002/aic.690371007.
- [26] R.F. Boyd, A.L. Zydney, Sieving characteristics of multilayer ultrafiltration membranes, J. Membr. Sci. 131 (1997) 155–165, https://doi.org/10.1016/S0376-7389(77)00045
- [27] A. Giacobbo, A.M. Bernardes, M.J.F. Rosa, M.N. De Pinho, Concentration polarization in ultrafiltration/nanofiltration for the recovery of polyphenols from

- winery wastewaters, Membranes 8 (3) (2018), https://doi.org/10.3390/
- [28] M. Hartinger, H.J. Heidebrecht, S. Schiffer, J. Dumpler, U. Kulozik, Milk protein fractionation by means of spiral-wound microfiltration membranes: effect of the pressure adjustment mode and temperature on flux and protein permeation, Foods 8 (6) (2019) 1–17, https://doi.org/10.3390/foods8060180.
- [29] T. Steinhauer, W. Kühnl, U. Kulozik, Impact of protein interactions and transmembrane pressure on physical properties of filter cakes formed during filtrations of skim milk, Procedia Food Science 1 (Icef 11) (2011) 886–892, https:// doi.org/10.1016/j.profoo.2011.09.134.
- [30] V. Aguirre Montesdeoca, A. Van der Padt, R.M. Boom, A.E.M. Janssen, Modelling of membrane cascades for the purification of oligosaccharides, J. Membr. Sci. 520 (2016) 712–722, https://doi.org/10.1016/j.memsci.2016.08.031.
- [31] Z. Rizki, A.E.M. Janssen, A. van der Padt, R.M. Boom, Separation of fructose and glucose via nanofiltration in presence of fructooligosaccharides, Membranes 10 (10) (2020) 1–11, https://doi.org/10.3390/membranes10100298.
- [32] M. Corredig, P.K. Nair, Y. Li, H. Eshpari, Z. Zhao, Invited review: understanding the behavior of caseins in milk concentrates, J. Dairy Sci. 102 (6) (2019) 4772–4782, https://doi.org/10.3168/jds.2018-15943.
- [33] J.N. De Wit, Nutritional and functional characteristics of whey proteins in food products, J. Dairy Sci. 81 (3) (1998) 597–608, https://doi.org/10.3168/jds.S0022-0302(98)75613-9.
- [34] H.J. Heidebrecht, J. Toro-Sierra, U. Kulozik, Concentration of immunoglobulins in microfiltration permeates of skim milk: impact of transmembrane pressure and temperature on the IgG transmission using different ceramic membrane types and pore sizes, Foods 7 (7) (2018), https://doi.org/10.3390/foods7070101.
- [35] A.D. Marshall, P.A. Munro, G. Trägårdh, Influence of permeate flux on fouling during the microfiltration of β-lactoglobulin solutions under cross-flow conditions, J. Membr. Sci. 130 (1–2) (1997) 23–30, https://doi.org/10.1016/S0376-7388(97) 00004-5.
- [36] E. Bijl, R. de Vries, H. van Valenberg, T. Huppertz, T. van Hooijdonk, Factors influencing casein micelle size in milk of individual cows: genetic variants and glycosylation of κ -casein, Int. Dairy J. 34 (1) (2014) 135–141, https://doi.org/10.1016/j.idairyj.2013.08.001.
- [37] C. Kürzl, U. Kulozik, Influence of pulsed and alternating flow on the filtration performance during skim milk microfiltration with flat-sheet membranes, Separ. Purif. Technol. 321 (April) (2023) 124234, https://doi.org/10.1016/j. seppur.2023.124234.
- [38] D. Roy, A. Ye, P.J. Moughan, H. Singh, Gelation of milks of different species (dairy cattle, goat, sheep, red deer, and water buffalo) using glucono-8-lactone and pepsin, J. Dairy Sci. 103 (7) (2020) 5844–5862, https://doi.org/10.3168/jds.2019-17571.
- [39] B.Y.J.D. Ferry, Scales for expressing membrane porosity, J. Gen. Physiol. 5 (1935) 95–104.
- [40] Q. Yao, C. Ji, C. He, S. Zhou, A hybrid experiment/theory method for soil conditioning in sandy cobble strata with large cobbles and boulders, Bull. Eng. Geol. Environ. (2021) 8189–8209, https://doi.org/10.1007/s10064-021-02418-9
- [41] A. Artemi, G.Q. Chen, S.E. Kentish, J. Lee, The relevance of critical flux concept in the concentration of skim milk using forward osmosis and reverse osmosis, J. Membr. Sci. 611 (June) (2020) 118357, https://doi.org/10.1016/j. memsci.2020.118357.
- [42] A.J. Sodt, R.W. Pastor, The tension of a curved surface from simulation, J. Chem. Phys. 137 (23) (2012) 1–12, https://doi.org/10.1063/1.4769880.
 [43] C. Degoulet, J.P. Busnel, J.F. Tassin, Study of the steric partition coefficient in size-
- [43] C. Degoulet, J.P. Busnel, J.F. Tassin, Study of the steric partition coefficient in size exclusion chromatography by Monte Carlo simulation, Polymer 35 (9) (1994) 1957–1962, https://doi.org/10.1016/0032-3861(94)90988-1.
- [44] A.A. Hussain, S.K. Nataraj, M.E.E. Abashar, I.S. Al-Mutaz, T.M. Aminabhavi, Prediction of physical properties of nanofiltration membranes using experiment and theoretical models, J. Membr. Sci. 310 (1–2) (2008) 321–336, https://doi.org/ 10.1016/j.memsci.2007.11.005.
- [45] A. Szymczyk, P. Fievet, Investigating transport properties of nanofiltration membranes by means of a steric, electric and dielectric exclusion model, J. Membr. Sci. 252 (1–2) (2005) 77–88, https://doi.org/10.1016/j.memsci.2004.12.002.
- [46] P. Bacchin, D. Si-Hassen, V. Starov, M.J. Clifton, P. Aimar, A unifying model for concentration polarization, gel-layer formation and particle deposition in crossflow membrane filtration of colloidal suspensions, Chem. Eng. Sci. 57 (1) (2002) 77–91, https://doi.org/10.1016/S0009-2509(01)00316-5.
- [47] S. Kimwra, Transport phenomena in membrane separation processes, J. Chem. Eng. Jpn. 25 (5) (1992) 469–480, https://doi.org/10.1252/jcej.25.469.
- [48] A.V. Smirnov, S.G. Ponomarev, V.P. Tarasovskii, V.V. Rybal'chenko, A.A. Vasin, V. V. Belov, Hard-sphere close-packing models: possible applications for developing promising ceramic and refractory materials, Glass Ceram. 75 (9–10) (2019) 345–351, https://doi.org/10.1007/s10717-019-00083-9 (Review).
- [49] C.L. Astudillo-Castro, Limiting flux and critical transmembrane pressure determination using an exponential model: the effect of concentration factor, temperature, and cross-flow velocity during casein micelle concentration by microfiltration, Ind. Eng. Chem. Res. 54 (1) (2015) 414–425, https://doi.org/ 10.1021/ic5033292
- [50] R. Tuinier, C.G. De Kruif, Stability of casein micelles in milk, J. Chem. Phys. 117(3) (2002) 1290–1295, https://doi.org/10.1063/1.1484379.
- [51] H.J. Heidebrecht, U. Kulozik, Fractionation of casein micelles and minor proteins by microfiltration in diafiltration mode. Study of the transmission and yield of the immunoglobulins IgG, IgA and IgM, Int. Dairy J. 93 (2019) 1–10, https://doi.org/ 10.1016/j.idairyj.2019.01.009.
- [52] W. Du, N. Quan, P. Lu, J. Xu, W. Wei, L. Zhang, Experimental and statistical analysis of the void size distribution and pressure drop validations in packed beds,

- Chem. Eng. Res. Des. 106 (2016) 115–125, https://doi.org/10.1016/j.
- [53] P. Qu, G. Gésan-Guiziou, A. Bouchoux, Dead-end filtration of sponge-like colloids: the case of casein micelle, J. Membr. Sci. 417–418 (2012) 10–19, https://doi.org/ 10.1016/j.memsci.2012.06.003.
- [54] L.E. Coppola, M.S. Molitor, S.A. Rankin, J.A. Lucey, Comparison of milk-derived whey protein concentrates containing various levels of casein, Int. J. Dairy Technol. 67 (4) (2014) 467–473, https://doi.org/10.1111/1471-0307.12157.
- [55] O. Mahony, I. James, A.O. Mahony, I.E.K.E. Smith, Purification of beta casein from milk, Patent 11/272,331 (US 2014/8889208 B2) 2 (12) (2014).
- [56] Y. Zhang, D. Liu, X. Liu, F. Hang, P. Zhou, J. Zhao, H. Zhang, W. Chen, Effect of temperature on casein micelle composition and gelation of bovine milk, Int. Dairy J. 78 (2018) 20–27, https://doi.org/10.1016/j.idairyj.2017.10.008.